SCIENTIFIC REPORTS

OPEN

CONFERENCE PROCEEDINGS

APEnergy2014

SUBJECT AREAS:
POROUS MATERIALS
SYNTHESIS AND PROCESSING
BATTERIES
NANOPARTICLES

Received
11 February 2014

Accepted
11 July 2014

Published
29 August 2014

Correspondence and requests for materials should be addressed to Y.C.K. (yckang@konkuk.ac.kr)

Electrochemical properties of yolk-shell structured $ZnFe_2O_4$ powders prepared by a simple spray drying process as anode material for lithium-ion battery

Jong Min Won, Seung Ho Choi, Young Jun Hong, You Na Ko & Yun Chan Kang

Department of Chemical Engineering, Konkuk University, 1 Hwayang-dong, Gwangjin-gu, Seoul 143-701, Korea.

$ZnFe_2O_4$ yolk–shell powders were prepared by applying a simple spray-drying process. Dextrin was used as a drying additive and carbon source material, and thus played a key role in the preparation of the powders. The combustion of precursor powders consisting of zinc and iron salts and dextrin obtained by a spray-drying process produced the yolk–shell-structured $ZnFe_2O_4$ powders even at a low post-treatment temperature of 350°C. The $ZnFe_2O_4$ powders prepared from the spray solution without dextrin had a filled and pockmarked structure. The initial discharge capacities of the $ZnFe_2O_4$ yolk–shell and filled powders post-treated at 450°C at a current density of 500 mA g^{-1} were 1226 and 993 mA h g^{-1}, respectively, and the corresponding initial Coulombic efficiencies were 74 and 58%. The discharge capacities of the $ZnFe_2O_4$ powders with yolk–shell and filled structures post-treated at 450°C after 200 cycles were 862 and 332 mA h g^{-1}, respectively. The $ZnFe_2O_4$ yolk–shell powders with high structural stability during cycling had superior electrochemical properties to those of the powders with filled structure.

Binary transition-metal oxides with spinel-like structures such as AB_2O_4 (A: Zn, Ni, Cu, B: Co, Mn, Fe) have been extensively researched for lithium-ion batteries (LIBs) because of their high reversible capacities[1–10]. The superior electrochemical properties of nanostructured binary transition-metal oxides prepared by liquid-solution and gas-phase reaction methods have been reported[2–11]. Yolk–shell powders with a distinctive core/void/shell configuration in particular have been studied as anode materials for LIBs because of their structural stability and good electrochemical properties at high current densities[8–16]. In recent studies, a spray pyrolysis process was applied to prepare various types of metal oxide powders with yolk–shell structures directly[16–18]. Yolk–shell-structured single and binary metal oxides have shown superior electrochemical properties even at high current densities[8–18].

In this manuscript, a large-scale production method of fabricating binary transition-metal oxide yolk–shell powders by applying a simple spray-drying process is proposed. In the spray-drying process, decomposition of metal salts does not occur because of the low operating temperature. Therefore, the spray-drying process is quite different from the spray pyrolysis process previously used to prepare yolk–shell powders of various compositions. However, one-pot preparation of yolk–shell powders cannot be achieved in a spray-drying process. Carbon is an inevitable requirement for the fabrication of yolk–shell powders using either the spray-drying process or the spray pyrolysis process. The key issue in spray drying is the need to prepare low-hygroscopicity precursor powders with a dense structure and spherical shape by applying an appropriate carbon source material. The carbon source material thus plays a key role in the preparation of yolk–shell-structured materials using the spray-drying process. Nanostructured zinc ferrite ($ZnFe_2O_4$) powders with various morphologies have been well studied as anode materials for LIBs[19–26]. However, the electrochemical properties of $ZnFe_2O_4$ yolk–shell powders have not been reported. In this study, dextrin was applied as both a carbon source material and drying agent for the large-scale production of $ZnFe_2O_4$ yolk–shell powders. The combustion of the precursor powders obtained by spray drying produced a yolk–shell-structured $ZnFe_2O_4$ powder with good electrochemical properties.

Results

The morphologies of the powders prepared directly by the spray-drying process from spray solutions with and without dextrin are shown in Figure 1. The dried powder particles exhibited a spherical shape and no aggregation

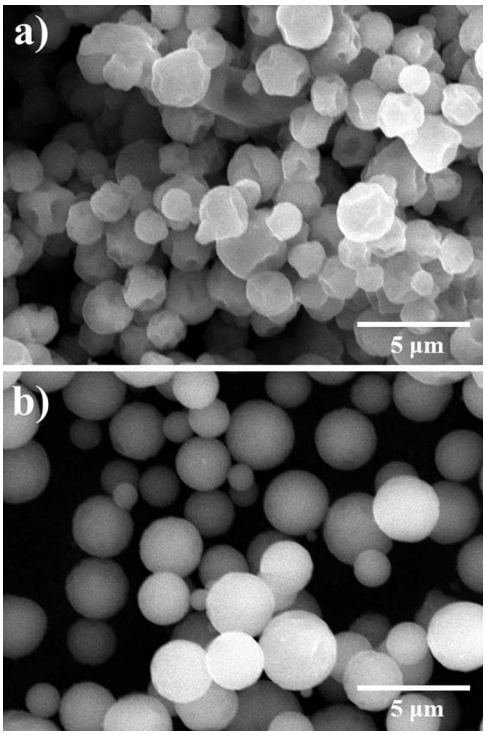

Figure 1 | SEM images of the as-prepared powders prepared from the spray solutions without and with dextrin: (a) without dextrin and (b) with dextrin.

regardless of drying additive because of the good drying characteristics of zinc and iron salts under high humidity conditions. However, the use of dextrin as both a drying additive and a carbon source material improved the smoothness of the surface of the precursor powders. The concentration gradient within the droplets due to fast drying produced precursor powders with a distorted spherical shape, as shown in Figure 1a. Figure S1 shows the thermogravimetric (TG) curve of the powders prepared from the spray solution with dextrin before and after post-treatment at 450°C. The precursor powders exhibited a distinct three-step weight loss below 400°C as a result of the decomposition of the metal salts and dextrin. The total weight loss of the precursor powders was 76 wt%. On the other hand, there was no observed weight loss in the powders post-treated at 450°C below 800°C.

Figure 2 shows the morphologies of the post-treated $ZnFe_2O_4$ powders. The $ZnFe_2O_4$ powders prepared without dextrin had similar morphology before and after post-treatment at 450°C, as shown in Figures 1a and 2a. The pockmarked, spherical shape of the precursor powders without dextrin was maintained even after decomposition of the zinc and iron salts to form the $ZnFe_2O_4$ powder. On the other hand, the morphology of the powders prepared with dextrin changed after post-treatment at temperatures above 350°C. The filled structure of the precursor powders changed into a yolk–shell structure with a core/void/shell configuration after post-treatment, as shown in the SEM and TEM images in Figures 2b–f. The TEM images of the $ZnFe_2O_4$ powders post-treated at 450°C clearly show a minimum of two shells in each particle. The elemental mapping images of the $ZnFe_2O_4$ yolk–shell powders post-treated at 450°C (Figure 2g) show the uniform distribution of Zn and Fe components all over the powder. The BET surface areas of the $ZnFe_2O_4$ powders with yolk-shell and filled structures post-treated at 450°C were 21.7 and 3.3 $m^2\ g^{-1}$, respectively.

Figure S2 shows the XRD patterns of the post-treated $ZnFe_2O_4$ powders. The post-treated powders had a pure $ZnFe_2O_4$ phase with no impurity phases irrespective of dextrin additive. Phase separation

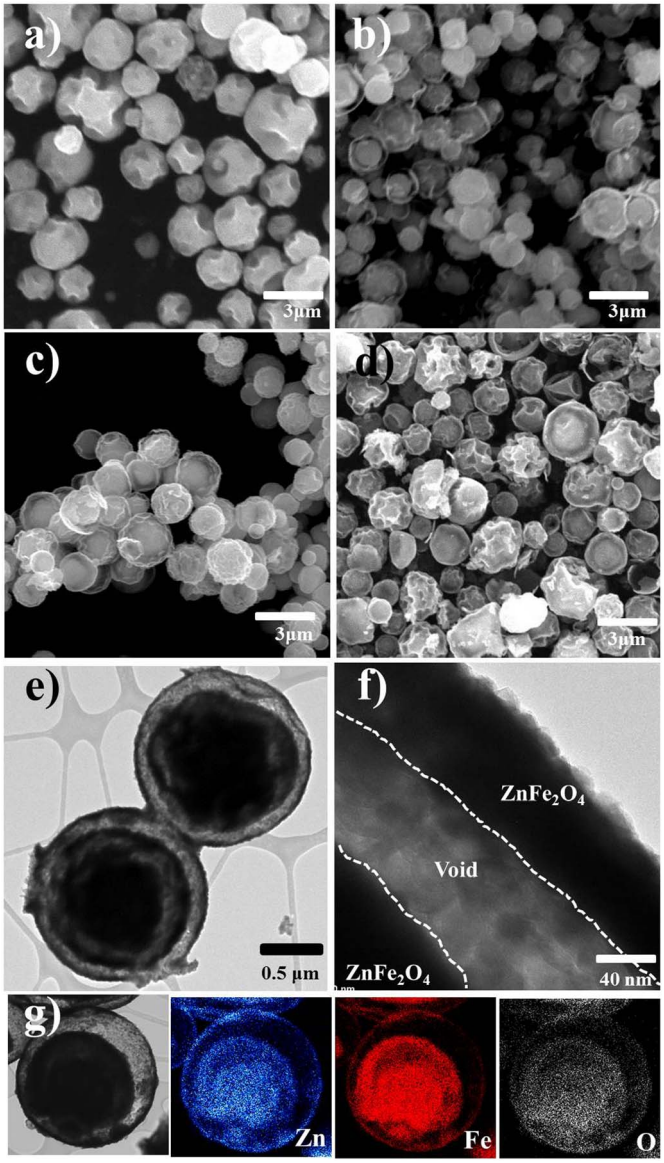

Figure 2 | SEM, TEM, and elemental mapping images of the $ZnFe_2O_4$ powders post-treated at various temperatures: (a) without dextrin, 450°C, (b) with dextrin, 350°C, (c) with dextrin, 400°C, (d–f) with dextrin, 450°C, and (g) elemental mapping images.

of each metal component could have occurred during the post-treatment process for the yolk–shell powders or during the spray-drying process for the precursor powders. However, phase separation of the zinc and iron components did not occur in the preparation process of the $ZnFe_2O_4$ powders. Therefore, phase-pure $ZnFe_2O_4$ yolk–shell powders were prepared even at a low post-treatment temperature of 350°C. The morphologies of the powders prepared from the spray solution with dextrin and post-treated at 200°C are shown in Figure S3. The powders post-treated at 200°C within an alumina boat were divided into two regions, one dark brown and the other black as shown by photograph in Figure S3. The precursor powders directly prepared by the spray-drying process and the phase-pure $ZnFe_2O_4$ yolk–shell powders were yellow and dark brown, respectively. The SEM images in Figures S4a and S4b show the morphologies of the black and dark brown powders, respectively. The dark brown powder had a yolk–shell structure, whereas the black powder had a filled structure. The carbonization of dextrin produced black Zn–Fe–C composite powders as an intermediate product during the post-treatment process. The repeated combustion and contraction processes of

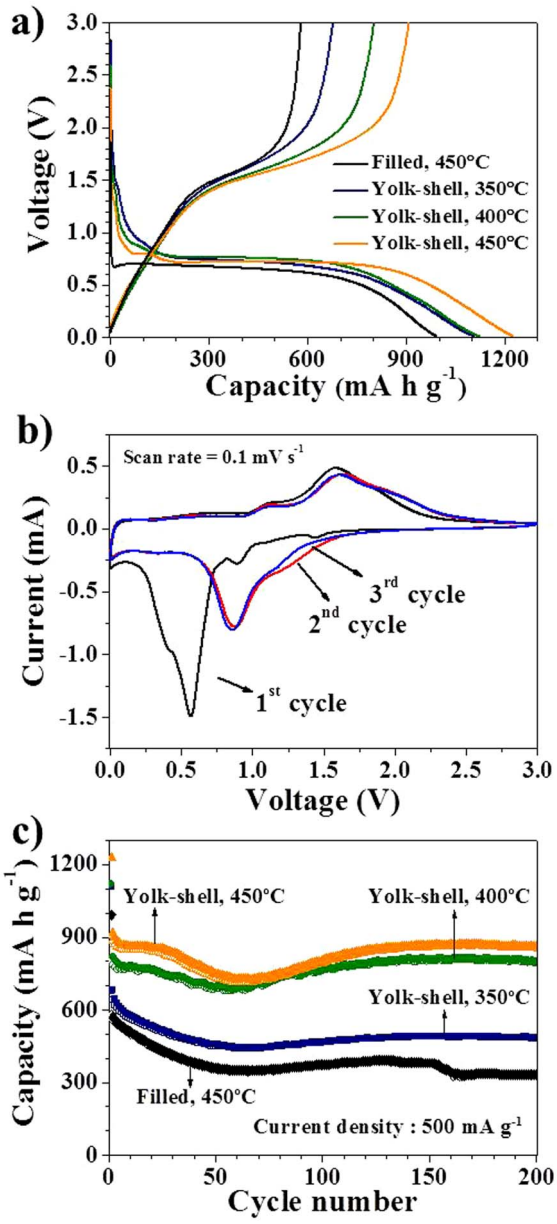

Figure 3 | Electrochemical properties of the $ZnFe_2O_4$ powders prepared from the spray solutions with and without dextrin: (a) initial charge and discharge curves, (b) cyclic voltammogram curves, and (c) cycling performances at a current density of 500 mA g^{-1}.

the Zn–Fe–C composite intermediate product formed during the post-treatment process produced the dark brown $ZnFe_2O_4$ yolk–shell powders.

The electrochemical properties of the $ZnFe_2O_4$ yolk–shell powders were compared with those of the powders with filled structure, and the results are shown in Figure 3. The $ZnFe_2O_4$ yolk–shell powders had similar initial discharge and charge curves at a current density of 500 mA g^{-1}, irrespective of post-treatment temperature. Obvious voltage plateaus, including a short one at 1.0 V and a long one at 0.75 V, were observed in the initial discharge curves. The short voltage plateau at approximately 1.0 V can be attributed to the formation of $Li_{1.5}ZnFe_2O_4$[19–21]. The subsequent long-voltage plateau corresponds to the decomposition of $ZnFe_2O_4$ into Zn and Fe metallic nanoparticles dispersed in the amorphous matrix of Li_2O[19–26]. On the other hand, the initial discharge curve of the $ZnFe_2O_4$ powders with filled structure had only a long plateau at 0.67 V. The initial discharge and charge capacities of the $ZnFe_2O_4$ yolk–shell powders post-treated at 450°C were 1226 and 909 mA h g^{-1}, respectively, and the corresponding initial Coulombic efficiency was 74%. On the other hand, the initial discharge and charge capacities of the $ZnFe_2O_4$ powders with filled morphology post-treated at 450°C were low as 993 and 580 mA h g^{-1}, respectively, and the corresponding initial Coulombic efficiency was 58%. The irreversible capacity losses for the initial cycles, as shown in Figure 3a, were mainly due to the formation of a solid electrolyte interface (SEI) layer at the electrode/electrolyte interface caused by the reduction of the electrolyte[19–26]. In addition, the structural destroy of the powders during the first cycle lowered the initial Coulombic efficiency of the $ZnFe_2O_4$ powders with filled structure. The $ZnFe_2O_4$ yolk–shell powders post-treated at a low temperature of 350°C also had a low initial Coulombic efficiency of 61% due to structural instability during cycling.

Figure 3b shows the cyclic voltammograms (CVs) of the $ZnFe_2O_4$ yolk–shell powders post-treated at 450°C for the first three cycles in the voltage range of 0.01–3.0 V versus Li/Li^+ at a scan rate of 0.1 mV s^{-1}. Upon the initial cathodic reaction, in which the voltage slope ranged from 1.5 to 0.8 V, the $ZnFe_2O_4$ phase transformed to the $Li_{1.5}ZnFe_2O_4$ phase[19–21]. The broad reduction peak at 0.55 V in the first cycle could be ascribed to the reduction of Fe^{3+} and Zn^{2+} to Fe^0 and Zn^0, respectively, as well as the formation of Li–Zn alloys and Li_2O[19–21]. In the subsequent cycles, one broad reduction peak, located at 0.9 V, was observed, which corresponds to the reversible reduction reaction of amorphous Fe_2O_3 and ZnO[27,28]. During the anodic process, two oxidation peaks are observed at 1.55 V and 1.8 V, which are associated with the oxidation of Zn^0 and Fe^0 to Zn^{2+} and Fe^{3+}, respectively[19–21]. From the second cycle onward, the cathodic and anodic peaks in the CV tests overlapped substantially, indicating that the electrode of the $ZnFe_2O_4$ yolk–shell powders showed outstanding cycle ability for the insertion and extraction of Li ions.

Figure 3c shows the cycling performances of the $ZnFe_2O_4$ powders at a current density of 500 mA g^{-1}. The $ZnFe_2O_4$ yolk-shell powders post-treated at 400 and 450°C had high discharge capacities of 800 and 862 mA h g^{-1} after 200 cycles. On the other hand, the $ZnFe_2O_4$ powders with filled structure post-treated at 450°C and the yolk–shell powders post-treated at 350°C had low discharge capacities of 332 and 484 mA h g^{-1} after 200 cycles, respectively, due to structural instability during cycling at a high current density. During cycling, the discharge capacities of the $ZnFe_2O_4$ yolk–shell powders post-treated at 400 and 450°C increased gradually after 60th cycles, primarily owing to the formation of a polymeric gel-like film on the active materials[15,29,30]. The polymeric gel-like film was also formed on the high BET surface area of the $ZnFe_2O_4$ yolk–shell powders post-treated 350°C. However, the increase in the discharge capacity as a result of the formation of a polymeric gel-like film on the active material was diminished by the decreased capacity due to the structural destroy of the yolk–shell powders post-treated at 350°C.

The structural stabilities of the $ZnFe_2O_4$ powders post-treated at 450°C during cycling were determined by electrochemical impedance spectroscopy (EIS) measurements and the results are shown in Figures 4a and 4b. Impedance measurements were carried out at room temperature on cells before cycling and after 50 cycles in the potential range of 0.01–3.0 V at a current density of 500 mA g^{-1}. The Nyquist plots of the electrodes were composed of a semicircle in the medium frequency region and an inclined line at low frequencies. The medium-frequency semicircle was assigned to the charge-transfer resistance, and the line inclined at ~45° to the real axis corresponded to the lithium diffusion process within the electrodes[31–33]. The charge transfer resistance of the $ZnFe_2O_4$ yolk–shell powders was much higher than that of the $ZnFe_2O_4$ filled powders, as shown in Figure 4a. The high contact area between the active material and electrolyte resulted in the high charge transfer resistance of the $ZnFe_2O_4$ yolk–shell powders with high surface area and enough void volume inside the powder for electrolyte penetration[16]. The charge

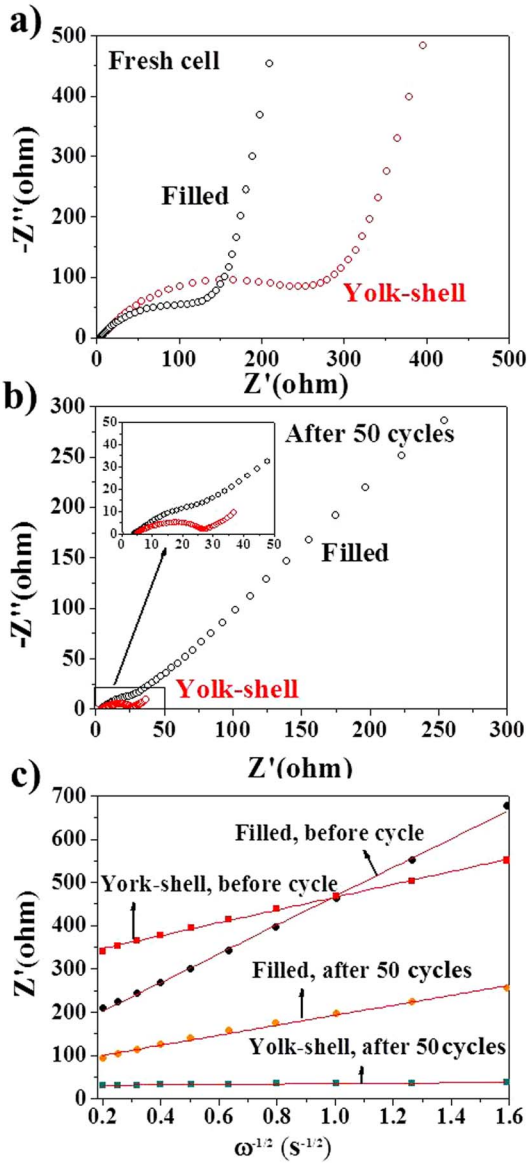

Figure 4 | Impedance analysis of the $ZnFe_2O_4$ powders prepared from the spray solutions with and without dextrin: (a) Nyquist impedance plots before cycle, (b) Nyquist impedance plots after 50 cycles, and (c) relationship between Z_{re} and $\omega^{-1/2}$ in the low-frequency region.

transfer resistances of the $ZnFe_2O_4$ powders with both yolk–shell and filled structures decreased after cycling because of the formation of an amorphous structure after cycling. The $ZnFe_2O_4$ yolk–shell powders had lower charge transfer resistance than the $ZnFe_2O_4$ powders with filled structure after 50 cycles, as shown in Figure 4b. Figure 4c shows the relationship between the real part of the impedance spectra (Z_{re}) and $\omega^{-1/2}$ (where ω is the angular frequency in the low-frequency region, $\omega = 2\pi f$) in the low-frequency region before cycling and after 50 cycles[31–33]. The low slope (σ, Warburg impedance coefficient) of the real part of Z_{re} versus $\omega^{-1/2}$ for the $ZnFe_2O_4$ yolk–shell powders reveals a higher lithium ion diffusion rate than the $ZnFe_2O_4$ powders with filled structure[31–33]. The low charge transfer resistance and high lithium ion diffusion rate of the $ZnFe_2O_4$ yolk–shell powders are due to their structural stability during cycling at a high current density. The slope of the $ZnFe_2O_4$ yolk–shell powders decreased after cycling (Figure 4c). The formation of a stable amorphous structure after cycling enhanced the Li^+ diffusion rate and facilitated rapid Li^+ charge/discharge of the $ZnFe_2O_4$ yolk–shell powders. Figures S5 and S6 show the morphology changes of the $ZnFe_2O_4$ powders with filled and yolk-shell structures after 50 cycles. The spherical shape of the powder with filled structure was destroyed after cycling as shown in the TEM images (Figure S5). However, the $ZnFe_2O_4$ yolk–shell powders maintained their spherical morphology even after cycling as shown in the field emission SEM and TEM images (Figure S6).

Discussion

A large-scale production method of fabricating binary transition-metal oxide yolk–shell powders by applying a simple spray-drying process was proposed. The preparation of precursor powders with low hygroscopicity, a dense structure, and a spherical shape by applying dextrin as an appropriate carbon source material was key to the preparation of these powders. The optimum post-treatment temperature to obtain the $ZnFe_2O_4$ yolk–shell powders with good electrochemical properties was 450°C. The $ZnFe_2O_4$ yolk–shell powders had higher initial discharge capacity and Coulombic efficiency and better cycling performance than the $ZnFe_2O_4$ powders with filled structure prepared by the same process. The structural stability of the $ZnFe_2O_4$ yolk–shell powders during cycling, a structure consisting of double shells and one core, enhanced the electrochemical properties of the $ZnFe_2O_4$ yolk–shell powders. The spray-drying process with a dextrin additive could be widely applied for large-scale production of multicomponent oxide materials with yolk–shell structures.

Methods

Material fabrication. A commercial spray-drying process was used to prepare powders with filled structure. Figure S7 shows a schematic diagram of the spray-drying process. The aqueous spray solution was prepared using zinc nitrate hexahydrate [$Zn(NO_3)_2{\cdot}6H_2O$], iron nitrate nonahydrate [$Fe(NO_3)_3{\cdot}9H_2O$], and dextrin [$(C_6H_{10}O_5)_n$]. The total concentration of the Zn and Fe components dissolved in distilled water was 0.1 M. The total amount of dextrin was fixed at 50 g L^{-1}. The spray solution containing a high concentration of the zinc and iron components was pumped into an atomizing device, where it was transformed into a spray of small droplets. A two-fluid nozzle was used as an atomizer, and the atomization pressure was 2.0 bar. These droplets were then brought into contact with a stream of hot air, which resulted in rapid evaporation of the moisture while the droplets were suspended in the drying air. The dry powder was separated from the humid air by centrifugal force in a cyclone system. The temperatures at the inlet and outlet of the spray dryer were 350°C and 120°C, respectively. The as-fabricated powders obtained by the spray-drying process, denoted herein as "precursor powders," were subsequently post-treated in air at temperatures between 350 and 450°C for 3 h.

Characterization. The crystal structures of the post-treated powders were determined by X-ray diffraction (XRD, X'pert PRO MPD) using Cu Kαradiation (λ = 1.5418 Å) at the Korea Basic Science Institute (Daegu). The morphological characteristics were investigated using scanning electron microscopy (SEM, JEOL JSM-6060) and high-resolution transmission electron microscopy (HRTEM, JEOL JEM-2100F) at 200 kV. The Brunauer–Emmett–Teller (BET) surface areas of the powders were measured using N_2 gas as an adsorbate. Thermogravimetric analysis (TGA, SDT Q600) was performed in air at a heating rate of 10°C min^{-1} to determine the decomposition characteristics of the precursor powders obtained by the spray-drying process.

Electrochemical measurements. The capacities and cycle properties of the powders were determined using a 2032-type coin cell. The electrode was prepared from a mixture comprising 70 wt% active material, 20 wt% activated carbon (Super P), and a 10 wt% sodium carboxymethyl cellulose (CMC) binder. Lithium metal and a microporous polypropylene film were used as the counter electrode and separator, respectively. The electrolyte was 1 M $LiPF_6$ in a 1 : 1 mixture (by volume) of ethylene carbonate–dimethyl carbonate (EC–DMC) with 5% fluoroethylene carbonate. Charge and discharge characteristics were determined by cycling from 0.01 to 3 V over a wide range of current densities. Cyclic voltammetry measurements were carried out at a scan rate of 0.1 mV s^{-1}.

1. Reddy, M. V., Rao, G. V. S. & Chowdari, B. V. R. Metal oxides and oxysalts as anode materials for Li ion batteries. *Chem. Rev.* **113**, 5364–5457 (2013).
2. Yuan, C. Z., Wu, H. B., Xie, Y. & Lou, X. W. Mixed transition-metal oxides: design, synthesis, and energy-related applications. *Angew. Chem. Int. Ed.* **53**, 1488–1504 (2014).

3. Courtel, F. M., Duncan, H., Abu-Lebdeh, Y. & Davidson, I. J. High capacity anode materials for Li-ion batteries based on spinel metal oxides AMn_2O_4 (A = Co, Ni, and Zn). *J. Mater. Chem.* **21**, 10206–10218 (2011).
4. Lavela, P. & Tirado, J. L. $CoFe_2O_4$ and $NiFe_2O_4$ synthesized by sol–gel procedures for their use as anode materials for Li ion batteries. *J. Power Sources* **172**, 379–387 (2007).
5. Sharma, Y., Sharma, N., Rao, G. V. S. & Chowdari, B. V. R. Nanophase $ZnCo_2O_4$ as a high performance anode material for Li-ion batteries. *Adv. Funct. Mater.* **17**, 2855–2861 (2007).
6. Hu, L., Zhong, H., Zheng, X. R., Huang, Y. M., Zhang, P. & Chen, Q. W. $CoMn_2O_4$ spinel hierarchical microspheres assembled with porous nanosheets as stable anodes for lithium-ion batteries. *Sci. Rep.* **2**, 986 (2012).
7. Wang, Y., Su, D., Ung, A., Ahn, J. & Wang, G. Hollow $CoFe_2O_4$ nanospheres as a high capacity anode material for lithium ion batteries. *Nanotechnology* **23**, 055402 (2012).
8. Li, J. F., Xiong, S. L., Liu, Y. R., Ju, Z. C. & Qian, Y. T. High electrochemical performance of monodisperse $NiCo_2O_4$ mesoporous microspheres as an anode material for Li-ion batteries. *ACS Appl. Mater. Interfaces* **5**, 981–988 (2013).
9. Zhang, G. Q., Yu, L., Wu, H. B., Hoster, H. E. & Lou, X. W. Formation of $ZnMn_2O_4$ ball-in-ball hollow microspheres as a high-performance anode for lithium-ion batteries. *Adv. Mater.* **24**, 4609–4613 (2012).
10. Zhou, L., Zhao, D. Y. & Lou, X. W. Double-shelled $CoMn_2O_4$ hollow microcubes as high-capacity anodes for lithium-Ion batteries. *Adv. Mater.* **24**, 745–748 (2012).
11. Yi, R., Feng, J., Lv, D., Gordin, M. L., Chen, S., Choi, D. & Wang, D. Amorphous Zn_2GeO_4 nanoparticles as anodes with high reversible capacity and long cycling life for Li-ion batteries. *Nano Energy* **2**, 498–504 (2013).
12. Jiang, J., Li, Y. Y., Liu, J. P., Huang, X. T., Yuan, C. Z. & Lou, X. W. Recent advances in metal oxide-based electrode architecture design for electrochemical energy storage. *Adv. Mater.* **24**, 5166–5180 (2012).
13. Zhang, X. F. *et al.* Facile synthesis of yolk–shell MoO_2 microspheres with excellent electrochemical performance as a Li-ion battery anode. *J. Mater. Chem. A* **1**, 6858–6864 (2013).
14. Wang, X. *et al.* Synthesis and lithium storage properties of Co_3O_4 nanosheet-assembled multishelled hollow spheres. *Adv. Funct. Mater.* **20**, 1680–1686 (2010).
15. Zhou, L. *et al.* Cheap and scalable synthesis of α-Fe_2O_3 multi-shelled hollow spheres as high-performance anode materials for lithium ion batteries. *Chem. Commun.* **49**, 8695–8697 (2013).
16. Choi, S. H. & Kang, Y. C. Yolk–shell, hollow, and single-crystalline $ZnCo_2O_4$ powders: preparation using a simple one-pot process and application in lithium-ion batteries. *ChemSusChem* **6**, 2111–2116 (2013).
17. Hong, Y. J., Son, M. Y. & Kang, Y. C. One-pot facile synthesis of double-shelled SnO_2 yolk-shell-structured powders by continuous process as anode materials for Li-ion batteries. *Adv. Mater.* **25**, 2279–2283 (2013).
18. Choi, S. H., Hong, Y. J. & Kang, Y. C. Yolk–shelled cathode materials with extremely high electrochemical performances prepared by spray pyrolysis. *Nanoscale* **5**, 7867–7871 (2013).
19. Bresser, D. *et al.* Carbon coated $ZnFe_2O_4$ nanoparticles for advanced lithium-ion anodes. *Adv. Energy Mater.* **3**, 513–523 (2013).
20. Guo, X. W. *et al.* Lithium storage in hollow spherical $ZnFe_2O_4$ as anode materials for lithium ion batteries. *Electrochem. Commun.* **12**, 847–850 (2010).
21. Yao, L. M. *et al.* A facile bubble-assisted synthesis of porous Zn ferrite hollow microsphere and their excellent performance as an anode in lithium ion battery. *J. Solid State Electrochem.* **17**, 2055–2060 (2013).
22. Ding, Y., Yang, Y. F. & Shao, H. X. High capacity $ZnFe_2O_4$ anode material for lithium ion batteries. *Electrochim. Acta* **56**, 9433–9438 (2011).
23. Mueller, F., Bresser, D., Paillard, E., Winter, M. & Passerini, S. Influence of the carbonaceous conductive network on the electrochemical performance of $ZnFe_2O_4$ nanoparticles. *J. Power Sources* **236**, 87–94 (2013).
24. Sui, J. *et al.* Facile synthesis of MWCNT–$ZnFe_2O_4$ nanocomposites as anode materials for lithium ion batteries. *J. Mater. Chem.* **22**, 13674–13681 (2012).
25. Deng, Y. F. *et al.* One-pot synthesis of $ZnFe_2O_4$/C hollow spheres as superior anode materials for lithium ion batteries. *Chem. Commun.* **47**, 6828–6830 (2011).
26. Xia, H., Qian, Y. Y., Fu, Y. S. & Wang, X. Graphene anchored with $ZnFe_2O_4$ nanoparticles as a high-capacity anode material for lithium-ion batteries. *Solid State Sci.* **17**, 67–71 (2013).
27. Cherian, C. T. *et al.* Electrospun α-Fe_2O_3 nanorods as a stable, high capacity anode material for Li-ion batteries. *J. Mater. Chem.* **22**, 12198–12204 (2012).
28. Huang, X. H., Xia, X. H., Yuan, Y. F. & Zhou, F. Porous ZnO nanosheets grown on copper substrates as anodes for lithium ion batteries. *Electrochim. Acta* **56**, 4960–4965 (2011).
29. Wu, Z. S. *et al.* Graphene anchored with Co_3O_4 nanoparticles as anode of lithium ion batteries with enhanced reversible capacity and cyclic performance. *ACS Nano* **4**, 3187–3194 (2010).
30. Choi, S. H., Lee, J. H. & Kang, Y. C. One-pot rapid synthesis of core–shell structured NiO@TiO_2 nanopowders and their excellent electrochemical properties as anode materials for lithium ion batteries. *Nanoscale* **5**, 12645–12650 (2013).
31. Ko, Y. N., Park, S. B., Jung, K. Y. & Kang, Y. C. One-pot facile synthesis of ant-cave-structured metal oxide−carbon microballs by continuous process for use as anode materials in Li-ion batteries. *Nano Lett.* **13**, 5462–5466 (2013).
32. Li, G. D., Xu, L. Q., Hao, Q., Wang, M. & Qian, Y. T. Synthesis, characterization and application of carbon nanocages as anode materials for high-performance lithium-ion batteries. *RSC Adv.* **2**, 284–291 (2012).
33. Shi, Y. *et al.* Hollow structured Li_3VO_4 wrapped with graphene nanosheets in situ prepared by a one-pot template-free method as an anode for lithium-ion batteries. *Nano Lett.* **13**, 4715–4720 (2013).

Acknowledgments

This work was supported by the National Research Foundation of Korea (NRF) grant funded by the Korea government (MEST) (No. 2012R1A2A2A02046367).

Author contributions

J.M.W., S.H.C. and Y.C.K. devised the concept, designed the experiment, and wrote the manuscript. J.M.W., S.H.C., Y.J.H. and Y.N.K. performed the experiments and analyzed the data. Y.C.K. supervised the project. All authors discussed the results and contributed in this manuscript.

Additional information

Supplementary information accompanies this paper at http://www.nature.com/scientificreports

Competing financial interests: The authors declare no competing financial interests.

How to cite this article: Won, J.M., Choi, S.H., Hong, Y.J., Ko, Y.N. & Kang, Y.C. Electrochemical properties of yolk-shell structured $ZnFe_2O_4$ powders prepared by a simple spray drying process as anode material for lithium-ion battery. *Sci. Rep.* **4**, 5857; DOI:10.1038/srep05857 (2014).